Multigap *s*-wave superconductivity emerging in the $1T'$ phase of $MoTe_2$ under hydrostatic pressure

Dongting Zhang,[1] Zhongchen Xu,[2] Tian Le,[1] Chufan Chen,[1,*] Ge Ye,[1] Fengrui Shi,[1] Shuaishuai Luo,[1] Youguo Shi,[2,3,4] and Xin Lu[1,5,†]

[1]*Center for Correlated Matter, School of Physics, Zhejiang University, Hangzhou 310058, China*
[2]*Beijing National Laboratory for Condensed Matter Physics, Institute of Physics, Chinese Academy of Sciences, Beijing 100190, China*
[3]*Center of Materials Science and Optoelectronics Engineering, University of Chinese Academy of Sciences, Beijing 100049, China*
[4]*Songshan Lake Materials Laboratory, Dongguan, Guangdong 523808, China*
[5]*Collaborative Innovation Center of Advanced Microstructures, Nanjing University, Nanjing, 210093, China*

(Received 11 September 2023; revised 22 February 2024; accepted 19 March 2024; published 5 April 2024)

Hydrostatic pressure transforms the superconductor $MoTe_2$ from a type-II Weyl semimetallic T_d phase to a topologically trivial $1T'$ phase at low temperature, serving as an ideal platform to explore the interplay between topology and superconductivity (SC). We report a soft point-contact-spectroscopy (SPCS) study on single-crystalline $MoTe_2$ under hydrostatic pressure up to 2.5 GPa, where the local SC transition temperature T_c of $MoTe_2$ in the contact region shows the same behavior as the reported pressure phase diagram. Excess current extracted from the integrated conductance subtracted by the normal state shows a positive correlation with the $1T'$ phase volume fraction as a function of pressure, supporting that the probed SC under pressure is mainly contributed by the $1T'$ phase of $MoTe_2$. Our SPCS spectra are better fitted by a two-gap *s*-wave Blonder-Tinkham-Klapwijk model in the whole pressure range, yielding $2\Delta_1/k_BT_c = 2.0$–2.5 and $2\Delta_2/k_BT_c = 4.15$–5.0, respectively, and suggesting a strong-coupling SC for $1T'$-$MoTe_2$.

DOI: 10.1103/PhysRevB.109.144506

I. INTRODUCTION

Topological superconductors (TSCs) have attracted considerable attention recently, since the Majorana zero mode at the edges obeys non-Abelian statistics and has a potential application in fault-tolerant quantum computations [1–3]. Intrinsic TSCs with spin-triplet pairing is rare in nature and one proposed route to realize TSC is to induce SC in topological materials by various tuning methods such as gating, doping, a proximity effect, high pressure, or local strain with hard tips [4–11], where the topology of the superconducting order parameter deserves careful discrimination. On the other hand, intrinsic superconducting materials with nontrivial topological bands, such as $PbTaSe_2$ [12–14], BiPd [15–18], and $2M$-WS_2 [19], serve as promising TSC candidates and call for careful investigations. Among them, T_d-$MoTe_2$ has been claimed to be a type-II Weyl semimetal without inversion symmetry at low temperatures, and a first-order structural transition at $T_s \sim 250$ K marks the transition from a topologically trivial $1T'$ phase to the T_d phase [20]. Topological Fermi arcs in T_d-$MoTe_2$ have been directly observed by angle-resolved photoemission spectroscopy (ARPES) measurements, and a topologically nontrivial π Berry phase has been observed in the Shubnikov–de Haas oscillations [21–26]. Meanwhile, a bulk superconductivity in T_d-$MoTe_2$ was discovered with a transition temperature $T_c = 0.1$ K, and several experiments have claimed it as a probable TSC [26–30]. However, such a low T_c makes it difficult to exactly determine the superconducting order parameter.

The SC in $MoTe_2$ is also susceptible to external tuning parameters such as doping, thickness, and pressure [20,31–33]. A substantially enhanced local T_c has been reported for point-contact spectroscopy (PCS) on $MoTe_2$ with either a sharp tip or silver epoxy at ambient pressure, and a maximum $T_c = 5$ K can be obtained, far beyond the bulk $T_c = 0.1$ K [28,29]. Such a behavior is reminiscent of PCS studies on CsV_3Sb_5, and has been argued due to a local strain effect from PCS [34]. Under hydrostatic pressure, its T_c is also enhanced with a T_c maximum of 8.2 K at 11.7 GPa, accompanied with a monotonic suppression of its structure transition up to a critical pressure $P_c \sim 1.1$ GPa [33]. In such a case, the SC in $MoTe_2$ should experience a change of band topology under pressure, and is an ideal platform to study the interplay between band topology and superconductivity. A two-band *s*-wave SC with possible $s\pm$ pairing was proposed for the T_d-$MoTe_2$ by both muon spin rotation/relaxation (μSR) measurements and theoretical calculations [30,35], but there is no direct evidence of a sign change. Soft PCS (SPCS) is in principle a powerful tool to probe the superconducting gap symmetry and can be easily extended to extreme conditions with hydrostatic pressure. SPCS has been successfully applied to several topological superconductor candidates under pressure, such as $PbTaSe_2$ and CsV_3Sb_5 [34,36,37], and it is thus desirable to explore the gap evolution and topological nature of SC in $MoTe_2$ under pressure [5,38].

*Corresponding author: cf.chen@nus.edu.sg
†Corresponding author: xinluphy@zju.edu.cn

In this paper, we have applied SPCS to study the pressure evolution of the SC gap for $MoTe_2$ from a topologically nontrivial to trivial phase. The local transition temperatures T_c^{SPCS} determined from SPCS are consistent with the bulk resistive T_c^R for pressure up to 2.5 GPa, and the excess current extracted from the integrated conductance subtracted by the normal state dramatically increases when the $1T'$ phase starts to emerge under pressure, supporting an intrinsic origin of the probed SC from the $1T'$ phase of $MoTe_2$. The differential conductance curves $G(V)$ for SPCS on $1T'$-$MoTe_2$ can be well described by a two-gap s-wave Blonder-Tinkham-Klapwijk (BTK) model under various pressures, and the SC gaps are in the strong-coupling limit.

II. EXPERIMENTAL METHODS

High-quality $MoTe_2$ single crystals were grown with tellurium flux as described elsewhere [39]. The SPCS measurement was achieved by attaching a 30-μm gold wire, with a drop of silver paint at the end, on a cleaved $MoTe_2$ sample. Point contacts of silver epoxy were coated by Stycast to secure the attachment, and the contact resistance was screened in the range of a few Ω to avoid the heating effect during a voltage scan. The $MoTe_2$ crystal was then mounted in a BeCu/NiCrAl hybrid piston-cylinder-type pressure cell with Daphne 7373 as the pressure transmitting medium. The pressure at low temperatures was calibrated by the superconducting transition temperature of Pb from electrical resistivity measurements while a Cernox sensor was attached directly on the pressure cell to determine its actual temperature. The SPCS differential conductance curve as a function of bias voltage $G(V)$ was recorded by the conventional lock-in technique in a quasi-four-probe configuration. An Oxford cryostat with a ^{3}He insert (base temperature 0.3 K) and dilution refrigerator insert (base temperature 0.1 K) was used for SPCS measurements under pressure.

III. RESULTS AND DISCUSSION

In order to check whether intrinsic superconductivity can be probed by SPCS for $MoTe_2$ under pressure, we have cross-checked the SC transition temperature T_c from both SPCS and electrical resistive measurements on the same sample S1 for comparison [see Supplemental Material (SM) [40] and Refs. [41–45] therein]. The pressure dependences of both T_c^{zero} and T_c^{onset} are consistent with earlier reports in Ref. [46] and the results are summarized as the color-filled region in its pressure phase diagram as in Fig. 1(b). As shown in Fig. S1(a) of the SM [40], the electrical resistance of the $MoTe_2$ single crystal does not show any resistive drop above 0.3 K below 0.5 GPa. The SC T_c abruptly increases above 0.5 GPa, where the $1T'$ phase starts to replace the T_d phase in $MoTe_2$ [46], and reaches 3.0–4.0 K at $P > 1.2$ GPa, where the $1T'$ phase has totally dominated $MoTe_2$ as in Fig. 1(b). In comparison, the differential conductance curves $G(V)$ from the point contact S1@1 barely show any Andreev reflection signal above 0.3 K for pressure $P < 0.5$ GPa as in Figs. S1(b) and S1(c). With increased pressure, the local T_c from SPCS can be identified as the kink for the temperature-dependent zero-bias conductance (ZBC) due to Andreev reflection, as marked by the red arrows

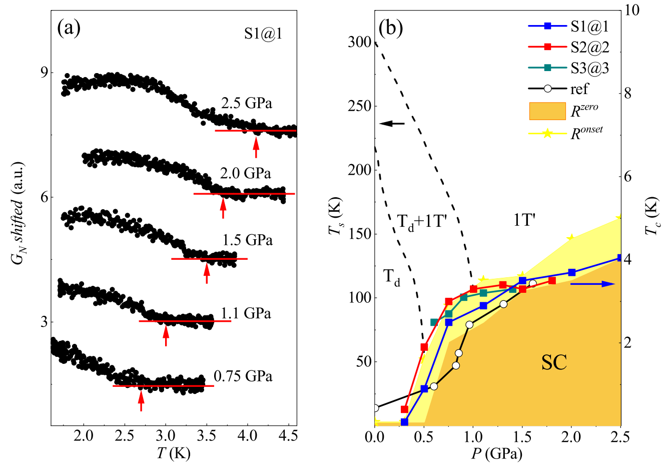

FIG. 1. (a) Normalized zero-bias conductance G_N as a function of temperature under various pressures, where the red arrows mark the local superconducting transition temperature T_c. (b) Temperature-pressure (T-P) phase diagram. Pressure evolution of local T_c from three distinct point contacts of SPCS, in comparison with the T_c determined from resistive measurements in Fig. S1(a) [40] and Ref. [46]. Its pressure-dependent structural transition temperatures T_s are adapted from Ref. [46] with three regions of T_d, $T_d + 1T'$, and $1T'$ in the phase diagram.

in Fig. 1(a). If we compare the local T_c for three sets of point contacts with the resistive T_c for the same sample under pressure as in Fig. 1(b), they show a consistent behavior as a function of pressure. The absence of a localized enhancement in T_c for SPCS under pressure provides evidence that an intrinsic superconducting state is probed across the entire pressure range up to 2.5 GPa, rather than the SC with a local-strain-induced T_c enhancement as previously reported at ambient pressure.

Figure 2(a) shows the pressure evolution of differential conductance curves $G(V)$ from the same contact S1@1 on $MoTe_2$ at the lowest temperature 0.3 K. We notice that the curves are nearly flat under pressure $P < 0.5$ GPa, indicating the absence of SC or a weak SC signal. However, at 0.7 GPa with the $1T'$ phase entering, an obvious double-peak structure in $G(V)$ is observed with a pronounced Andreev reflection amplitude, suggesting the emergence of SC only in the $1T'$ domains for $MoTe_2$ under pressure. The peak intensity then gradually grows with increased pressure, and finally saturates at around $P > 1.2$ GPa, where the $1T'$ phase totally occupies the bulk sample. Similar behavior was also present in the other two contacts S2@1 and S3@1 of SPCS as in Figs. S2(a) and S2(b) of the SM [40], which is in sharp contrast to the case of SPCS on CsV_3Sb_5 and $PbTaSe_2$, whose peak intensity is insensitive to pressure [34,36,37]. In order to quantitatively analyze the amplitude of the superconducting signal for SPCS on $MoTe_2$, we extract the SPCS excess current as a function of pressure, which is defined as the integration of the conductance subtracted by the normal-state baseline in the voltage range of $(-1, +1)$ mV and proportional to the SC volume in the contact region. Figure 2(b) shows the excess current for three distinct point contacts and they all start to grow near 0.5 GPa and finally become constant above 1.2 GPa, sharing a

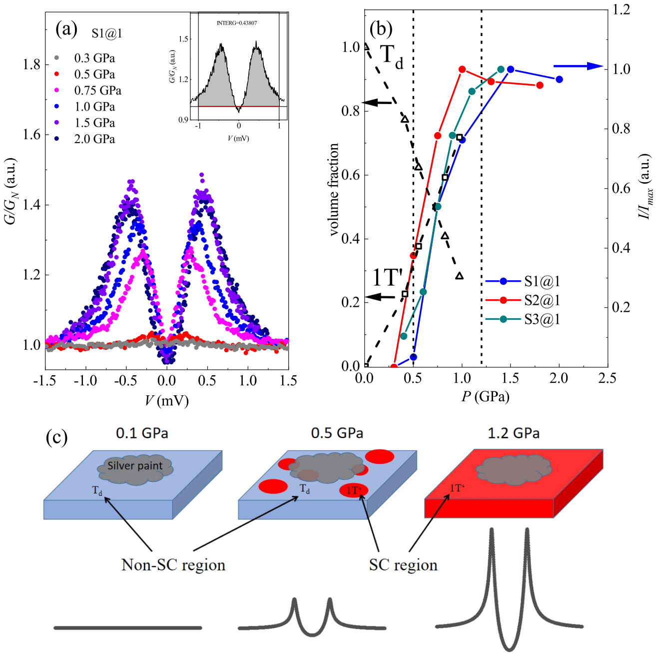

FIG. 2. (a) Normalized differential conductance curves $G(V)/G_N$ from point contact S1@1 under different pressures. (b) Pressure evolution of the excess currents for different point contacts signals the SC volume fraction in the contact region, in comparison with the $1T'$ phase volume fraction adapted from Ref. [46]. (c) Schematic illustration of a soft point contact on $MoTe_2$ under different pressures with increasing volume fraction of the $1T'$ phase (superconducting region) and thus excess current.

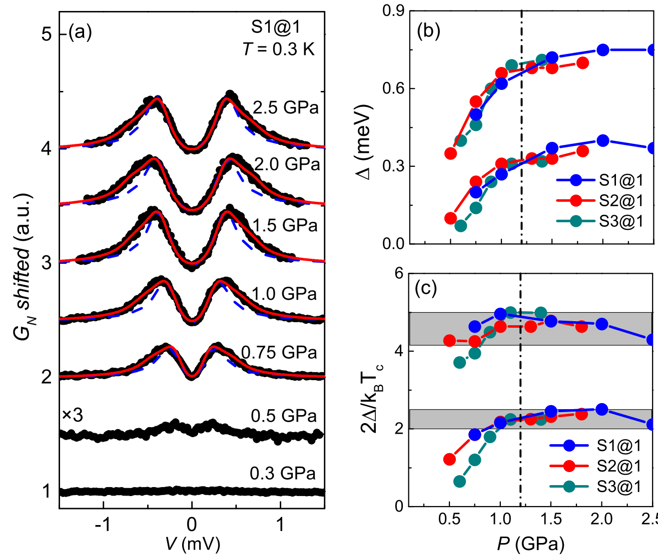

FIG. 3. (a) Pressure evolution of the normalized differential conductance curves $G_N(V)$ for point contacts S1@1 of SPCS, in comparison with the single-gap (blue lines) and two-gap (red lines) *s*-wave BTK fittings, where the curves are vertically shifted for clarity. (b) and (c) Pressure dependence of superconducting gaps and their $2\Delta/k_BT_c$ extracted from (a). The dashed line in (b) and (c) marks the critical pressure where $MoTe_2$ has completely entered into the $1T'$ phase.

common trend with pressure. The amplitude of excess current is exactly opposite to the volume fraction of the T_d phase, but shows a positive correlation with that of the $1T'$ phase under pressure as in Fig. 2(b). Figure 2(c) illustrates the evolution of the point-contact differential conductance curves with increased superconducting volume fraction as more of the $1T'$ phase transforms into the T_d phase in the contact area under pressure. Analogous to the inhomogeneous state with a phase separation of the normal state and superconductivity, as in the case of the mixed state in a magnetic field for the type-I superconductor $PdTe_2$ or type-II/1 superconductor $NbGe_2$ [47,48], our results support that the dominant SC under pressure arises from the topologically trivial $1T'$ phase and should be distinct from the SC in the topologically nontrivial T_d phase.

Figure 3 shows a series of normalized differential conductance curves $G_N(V)$ for the contact S1@1 at the lowest temperature $T = 0.3$ K under different pressures, which manifest a common double-peak feature. With increased pressure, the double peaks gradually shift to higher voltages and signal pressure-enhanced superconducting gap values. A single-gap *s*-wave BTK fitting obviously fails to reproduce the experimental data as illustrated by the blue dashed line in Fig. 3(a). Due to its multisheet Fermi surface with several hole and electron pockets [35], a trivial two-gap *s*-wave pairing BTK model with a slightly different gap magnitude has been considered for $MoTe_2$, where the conductance $G(V) = \omega G_1(V) + (1-\omega)G_2(V)$ has two components from separate gaps and the spectra weight ω is attributed to the smaller gap Δ_1. If we keep ω constant under various pressures, the $G(V)$ curves can be better fitted as shown by the red solid line in Fig. 3(a). The extracted gap values are plotted in Fig. 3(b) as a function of pressure, together with the other two point contacts S2@1 and S3@1 in a high consistency [their conductance and fitting curves are shown in Figs. S2(c) and S2(d) of the SM [40]]. Even though an anisotropic *s*-wave fitting would be comparable to the two-gap fitting as shown in Fig. S2(e) of the SM [40], a two-gap *s*-wave superconductivity in $1T'$-$MoTe_2$ under pressure seems favored, considering earlier theoretical proposals, a μSR report, and the μ_0H_{c2}-T phase diagram from ultralow transport measurements [28,30,35]. As in Fig. 3(b), the extracted gaps Δ_1 and Δ_2 gradually increase with pressure, while the ratio of the SC gap to the T_c, $2\Delta_1/k_BT_c = 2.0$–2.5 and $2\Delta_2/k_BT_c = 4.15$–5.0, favor a strong-coupling SC for the $1T'$-$MoTe_2$ as in Fig. 3(c), where the $2\Delta/k_BT_c$ of the smaller gap below the weak-coupling limit 3.52 is commonly observed. In the pressure range of (0.7, 1.2) GPa, a smaller $2\Delta/k_BT_c$ value compared with the one above 1.2 GPa is observed, and we speculate that the $1T'$ phase with higher T_c just partially occupies the sample and its superconductivity would be compromised with reduced SC gaps due to the proximity effect by its neighboring normal-state T_d phase with a substantial volume [49,50].

In order to characterize the temperature evolution of the SC gaps, we take the contact S1@1 for example and plot the temperature-dependent conductance curves $G(V)$ in Figs. 4(a) and 4(b) for SPCS at $P = 0.7$ GPa and $P = 2.0$ GPa, respectively. With increased temperatures, the double peaks gradually get smeared into a broad zero-bias peak, and finally disappear at their respective T_c. As shown by the red solid

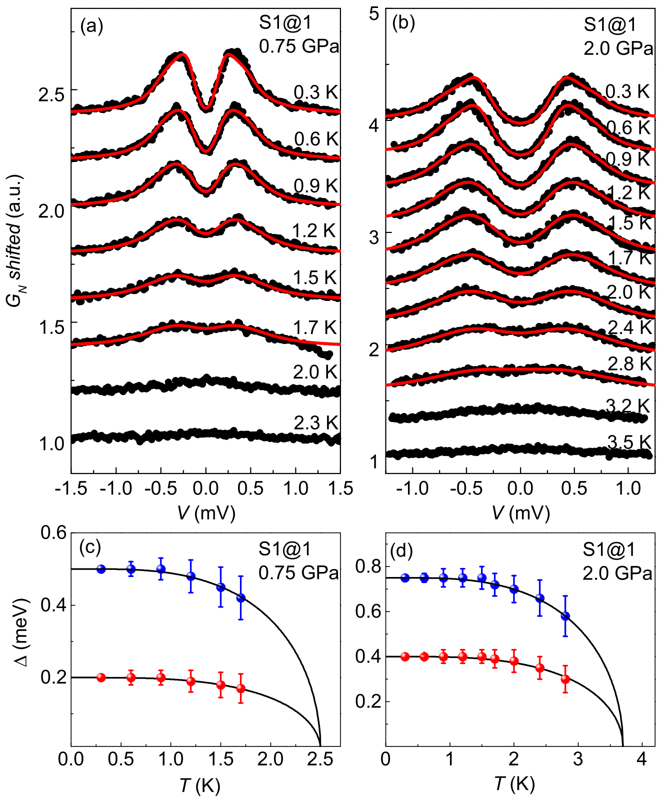

FIG. 4. (a) and (b) Temperature dependence of the normalized conductance curves $G_N(V)$ for point contact S1@1 at 0.75 and 2.0 GPa, respectively, in comparison with the two-gap *s*-wave BTK fitting curves (red lines), where the curves are vertically shifted for clarity. (c) and (d) The extracted superconducting gaps $\Delta_{1(2)}$ as a function of temperature from (a) and (b), respectively.

lines in Figs. 4(a) and 4(b), the conductance curves $G(V)$ can be well described by the two-gap *s*-wave BTK fitting, while the broad zero-bias peaks at high temperatures make it difficult to reliably extract Δ_1 and Δ_2. The obtained SC gaps Δ_1 and Δ_2 both follow a standard BCS temperature behavior as in Figs. 4(c) and 4(d), respectively, and we stress that the relation between a conventional multiband superconductor and its topologically trivial band nature for the $1T'$-$MoTe_2$ deserves more careful investigations for future studies under pressure.

As stated before, the local SC T_c can be significantly enhanced for SPCS on $MoTe_2$ at ambient pressure. However, such an effect is absent in most SPCS measurements under hydrostatic pressure, where intrinsic SC in the $1T'$-$MoTe_2$ has been probed instead, similar to the case of SPCS on CsV_3Sb_5. We would argue that such a dramatic T_c enhancement in $MoTe_2$ at ambient pressure might be ascribed to the local strain effect from the point contact itself, rather than due to its topologically nontrivial T_d phase [34,51]. A recent biaxial-strain study on $MoTe_2$ reports that its T_c can also be dramatically enhanced by fivefold, illustrating the strain sensitivity of $MoTe_2$ [51]. Such a local strain can tune the band structure and increase the carrier density near the Fermi level, resulting in a T_c enhancement [52]. In only a few trials, the local T_c enhancement is still present for SPCS on $MoTe_2$ at a low pressure as in Fig. S4 of SM [40], and the conductance curves show an obvious double-peak feature with an enhanced intensity below 0.5 GPa. However, a higher pressure would smear the SC first with reduced T_c and then track the intrinsic SC evolution under pressure. For comparison, the local T_c for PCS on $MoTe_2$ can be enhanced nearly 50 times by the sharp tip at ambient pressure and $MoTe_2$ seems to exhibit a higher strain sensitivity than CsV_3Sb_5 [28,29]. In such a case, a pronounced excess current has already been observed under low pressures as in Fig. S4(e) [40], evidencing a possible emergence of the $1T'$ phase induced by the local strain. We note that a uniaxial strain along the *a* axis is proposed to facilitate the T_d to $1T'$ structure transition in $MoTe_2$ [46,53]. Therefore, we speculate that the local strain induced by the SPCS might be partially or completely eliminated under hydrostatic pressure, and how the strain and pressure tune the $MoTe_2$ system deserve further experimental and theoretical studies.

IV. SUMMARY

In conclusion, we have systematically studied the superconductivity of $MoTe_2$ under pressure by SPCS measurements up to 2.5 GPa. The extrinsic T_c-enhancement behavior at ambient pressure from SPCS on $MoTe_2$ is absent under hydrostatic pressure, and an intrinsic SC is evidenced to emerge in the topologically trivial $1T'$ phase. A two-gap *s*-wave BTK model without a sign change can well fit the conductance curves $G(V)$ for $MoTe_2$ in the pressure range up to 2.5 GPa, and the superconducting gaps follow a standard BCS temperature behavior, yielding $2\Delta_1/k_BT_c = 2.0$–2.5 and $2\Delta_2/k_BT_c = 4.15$–5.0 for $1T'$-$MoTe_2$ in the strong-coupling limit.

ACKNOWLEDGMENTS

Our work was supported by the National Key Research & Development Program of China (Grants No. 2022YFA1402200 and No. 2017YFA0303101), the National Natural Science Foundation of China (Grants No. 12174333, No. U2032204, and No. U22A6005), the Strategic Priority Research Program of the Chinese Academy of Sciences (Grant No. XDB33010000), the Key R&D Program of Zhejiang Province, China (Grant No. 2021C01002), and Synergetic Extreme Condition User Facility (SECUF).

[1] M. Sato and Y. Ando, Topological superconductors: A review, Rep. Prog. Phys. **80**, 076501 (2017).
[2] M. Leijnse and K. Flensberg, Introduction to topological superconductivity and Majorana fermions, Semicond. Sci. Technol. **27**, 124003 (2012).
[3] A. Stern and N. H. Lindner, Topological quantum computation—from basic concepts to first experiments, Science **339**, 1179 (2013).
[4] E. Sajadi, T. Palomaki, Z. Fei, W. Zhao, P. Bement, C. Olsen, S. Luescher, X. Xu, J. A. Folk, and D. H. Cobden, Gate-induced

superconductivity in a monolayer topological insulator, Science **362**, 922 (2018).

[5] S. Sasaki, M. Kriener, K. Segawa, K. Yada, Y. Tanaka, M. Sato, and Y. Ando, Topological superconductivity in $Cu_xBi_2Se_3$, Phys. Rev. Lett. **107**, 217001 (2011).

[6] T. H. Hsieh and L. Fu, Majorana fermions and exotic surface Andreev bound states in topological superconductors: Application to $Cu_xBi_2Se_3$, Phys. Rev. Lett. **108**, 107005 (2012).

[7] P. Zhang, K. Yaji, T. Hashimoto, Y. Ota, T. Kondo, K. Okazaki, Z. Wang, J. Wen, G. D. Gu, H. Ding, and S. Shin, Observation of topological superconductivity on the surface of an iron-based superconductor, Science **360**, 182 (2018).

[8] L. Fu and C. L. Kane, Superconducting proximity effect and Majorana fermions at the surface of a topological insulator, Phys. Rev. Lett. **100**, 096407 (2008).

[9] V. Mourik, K. Zuo, S. M. Frolov, S. R. Plissard, E. P. A. M. Bakkers, and L. P. Kouwenhoven, Signatures of Majorana fermions in hybrid superconductor-semiconductor nanowire devices, Science **336**, 1003 (2012).

[10] M. J. Park, G. Sim, M. Y. Jeong, A. Mishra, M. J. Han, and S. Lee, Pressure-induced topological superconductivity in the spin–orbit Mott insulator $GaTa_4Se_8$, npj Quantum Mater. **5**, 41 (2020).

[11] H. Wang, H. Wang, H. Liu, H. Lu, W. Yang, S. Jia, X.-J. Liu, X. C. Xie, J. Wei, and J. Wang, Observation of superconductivity induced by a point contact on 3D Dirac semimetal Cd_3As_2 crystals, Nat. Mater. **15**, 38 (2016).

[12] M. N. Ali, Q. D. Gibson, T. Klimczuk, and R. J. Cava, Noncentrosymmetric superconductor with a bulk three-dimensional Dirac cone gapped by strong spin-orbit coupling, Phys. Rev. B **89**, 020505(R) (2014).

[13] S.-Y. Guan, P.-J. Chen, M.-W. Chu, R. Sankar, F. Chou, H.-T. Jeng, C.-S. Chang, and T.-M. Chuang, Superconducting topological surface states in the noncentrosymmetric bulk superconductor $PbTaSe_2$, Sci. Adv. **2**, e1600894 (2016).

[14] T. Le, Y. Sun, H.-K. Jin, L. Che, L. Yin, J. Li, G. Pang, C. Xu, L. Zhao, S. Kittaka, T. Sakakibara, K. Machida, R. Sankar, H. Yuan, G. Chen, X. Xu, S. Li, Y. Zhou, and XinLu, Evidence for nematic superconductivity of topological surface states in $PbTaSe_2$, Sci. Bull. **65**, 1349 (2020).

[15] M. Mondal, B. Joshi, S. Kumar, A. Kamlapure, S. C. Ganguli, A. Thamizhavel, S. S. Mandal, S. Ramakrishnan, and P. Raychaudhuri, Andreev bound state and multiple energy gaps in the noncentrosymmetric superconductor BiPd, Phys. Rev. B **86**, 094520 (2012).

[16] M. Neupane, N. Alidoust, M. M. Hosen, J.-X. Zhu, K. Dimitri, S.-Y. Xu, N. Dhakal, R. Sankar, I. Belopolski, D. S. Sanchez, T.-R. Chang, H.-T. Jeng, K. Miyamoto, T. Okuda, H. Lin, A. Bansil, D. Kaczorowski, F. Chou, M. Z. Hasan, and T. Durakiewicz, Observation of the spin-polarized surface state in a noncentrosymmetric superconductor BiPd, Nat. Commun. **7**, 13315 (2016).

[17] M. A. Khan, D. E. Graf, I. Vekhter, D. A. Browne, J. F. DiTusa, W. A. Phelan, and D. P. Young, Quantum oscillations and a nontrivial Berry phase in the noncentrosymmetric topological superconductor candidate BiPd, Phys. Rev. B **99**, 020507(R) (2019).

[18] X. Xu, Y. Li, and C. L. Chien, Spin-triplet pairing state evidenced by half-quantum flux in a noncentrosymmetric superconductor, Phys. Rev. Lett. **124**, 167001 (2020).

[19] Y. W. Li, H. J. Zheng, Y. Q. Fang, D. Q. Zhang, Y. J. Chen, C. Chen, A. J. Liang, W. J. Shi, D. Pei, L. X. Xu, S. Liu, J. Pan, D. H. Lu, M. Hashimoto, A. Barinov, S. W. Jung, C. Cacho, M. X. Wang, Y. He, L. Fu *et al.*, Observation of topological superconductivity in a stoichiometric transition metal dichalcogenide $2M$-WS_2, Nat. Commun. **12**, 2874 (2021).

[20] Y. Qi, P. G. Naumov, M. N. Ali, C. R. Rajamathi, W. Schnelle, O. Barkalov, M. Hanfland, S.-C. Wu, C. Shekhar, Y. Sun, V. Süß, M. Schmidt, U. Schwarz, E. Pippel, P. Werner, R. Hillebrand, T. Förster, E. Kampert, S. Parkin, R. J. Cava *et al.*, Superconductivity in Weyl semimetal candidate $MoTe_2$, Nat. Commun. **7**, 11038 (2016).

[21] Z. Wang, D. Gresch, A. A. Soluyanov, W. Xie, S. Kushwaha, X. Dai, M. Troyer, R. J. Cava, and B. A. Bernevig, $MoTe_2$: A type-II Weyl topological metal, Phys. Rev. Lett. **117**, 056805 (2016).

[22] J. Jiang, Z. Liu, Y. Sun, H. Yang, C. Rajamathi, Y. Qi, L. Yang, C. Chen, H. Peng, C.-C. Hwang, S. Sun, S.-K. Mo, I. Vobornik, J. Fujii, S. Parkin, C. Felser, B. Yan, and Y. Chen, Signature of type-II Weyl semimetal phase in $MoTe_2$, Nat. Commun. **8**, 13973 (2017).

[23] A. Tamai, Q. S. Wu, I. Cucchi, F. Y. Bruno, S. Riccò, T. K. Kim, M. Hoesch, C. Barreteau, E. Giannini, C. Besnard, A. A. Soluyanov, and F. Baumberger, Fermi arcs and their topological character in the candidate type-II Weyl semimetal $MoTe_2$, Phys. Rev. X **6**, 031021 (2016).

[24] L. Huang, T. M. McCormick, M. Ochi, Z. Zhao, M.-T. Suzuki, R. Arita, Y. Wu, D. Mou, H. Cao, J. Yan, N. Trivedi, and A. Kaminski, Spectroscopic evidence for a type II Weyl semimetallic state in $MoTe_2$, Nat. Mater. **15**, 1155 (2016).

[25] K. Deng, G. Wan, P. Deng, K. Zhang, S. Ding, E. Wang, M. Yan, H. Huang, H. Zhang, Z. Xu, J. Denlinger, A. Fedorov, H. Yang, W. Duan, H. Yao, Y. Wu, S. Fan, H. Zhang, X. Chen, and S. Zhou, Experimental observation of topological Fermi arcs in type-II Weyl semimetal $MoTe_2$, Nat. Phys. **12**, 1105 (2016).

[26] X. Luo, F. C. Chen, J. L. Zhang, Q. L. Pei, G. T. Lin, W. J. Lu, Y. Y. Han, C. Y. Xi, W. H. Song, and Y. P. Sun, T_d-$MoTe_2$: A possible topological superconductor, Appl. Phys. Lett. **109**, 102601 (2016).

[27] W. Wang, S. Kim, M. Liu, F. A. Cevallos, R. J. Cava, and N. P. Ong, Evidence for an edge supercurrent in the Weyl superconductor $MoTe_2$, Science **368**, 534 (2020).

[28] J. Luo, Y. Li, J. Zhang, H. Ji, H. Wang, J.-Y. Shan, C. Zhang, C. Cai, J. Liu, Y. Wang, Y. Zhang, and J. Wang, Possible unconventional two-band superconductivity in $MoTe_2$, Phys. Rev. B **102**, 064502 (2020).

[29] Y. Naidyuk, O. Kvitnitskaya, D. Bashlakov, S. Aswartham, I. Morozov, I. Chernyavskii, G. Fuchs, S.-L. Drechsler, R. Hühne, K. Nielsch, B. Büchner, and D. Efremov, Surface superconductivity in the Weyl semimetal $MoTe_2$ detected by point contact spectroscopy, 2D Mater. **5**, 045014 (2018).

[30] Z. Guguchia, F. von Rohr, Z. Shermadini, A. T. Lee, S. Banerjee, A. R. Wieteska, C. A. Marianetti, B. A. Frandsen, H. Luetkens, Z. Gong, S. C. Cheung, C. Baines, A. Shengelaya, G. Taniashvili, A. N. Pasupathy, E. Morenzoni, S. J. L. Billinge, A. Amato, R. J. Cava, R. Khasanov *et al.*, Signatures of the topological s^{+-} superconducting order parameter in the type-II Weyl semimetal T_d-$MoTe_2$, Nat. Commun. **8**, 1082 (2017).

[31] Y. Li, Q. Gu, C. Chen, J. Zhang, Q. Liu, X. Hu, J. Liu, Y. Liu, L. Ling, M. Tian, Y. Wang, N. Samarth, S. Li, T. Zhang, J.

Feng, and J. Wang, Nontrivial superconductivity in topological $MoTe_{2-x}S_x$ crystals, Proc. Natl. Acad. Sci. USA **115**, 9503 (2018).
[32] P. Li, J. Cui, J. Zhou, D. Guo, Z. Zhao, J. Yi, J. Fan, Z. Ji, X. Jing, F. Qu, C. Yang, L. Lu, J. Lin, Z. Liu, and G. Liu, Phase transition and superconductivity enhancement in Se-Substituted $MoTe_2$ thin films, Adv. Mater. **31**, 1904641 (2019).
[33] Y. J. Hu, Y. T. Chan, K. T. Lai, K. O. Ho, X. Guo, H.-P. Sun, K. Y. Yip, D. H. L. Ng, H.-Z. Lu, and S. K. Goh, Angular dependence of the upper critical field in the high-pressure $1T'$ phase of $MoTe_2$, Phys. Rev. Mater. **3**, 034201 (2019).
[34] D. Zhang, C. Chen, L. Yin, Y.-E. Huang, F. Shi, Y. Liu, X. Xu, H. Yuan, and X. Lu, Superconducting gap evolution of kagome metal CsV_3Sb_5 under pressure, Sci. China: Phys. Mech. Astron. **66**, 227411 (2023).
[35] H. Paudyal, S. Poncé, F. Giustino, and E. R. Margine, Superconducting properties of $MoTe_2$ from *ab initio* anisotropic Migdal-Eliashberg theory, Phys. Rev. B **101**, 214515 (2020).
[36] H. Zi, L.-X. Zhao, X.-Y. Hou, L. Shan, Z. Ren, G.-F. Chen, and C. Ren, Pressure-dependent point-contact spectroscopy of superconducting $PbTaSe_2$ single crystals, Chin. Phys. Lett. **37**, 097403 (2020).
[37] H. Zi, Y.-q. Zhao, M.-c. He, Y.-j. Long, L.-x. Zhao, X.-y. Hou, H.-x. Yang, Y.-f. Yang, L. Shan, Z.-a. Ren, J.-q. Li, J.-p. Hu, G.-f. Chen, P. Xiong, and C. Ren, Pressure-induced surface superconductivity in the noncentrosymmetric superconductor $PbTaSe_2$: Pressure-dependent point-contact Andreev spectroscopy, Phys. Rev. B **109**, 064510 (2024).
[38] G. J. Zhao, X. X. Gong, J. C. He, J. A. Gifford, H. X. Zhou, Y. Chen, X. F. Jin, C. L. Chien, and T. Y. Chen, Triplet *p*-wave superconductivity with ABM state in epitaxial Bi/Ni bilayers, arXiv:1810.10403.
[39] X. Jia, M. Wang, D. Yan, S. Xue, S. Zhang, J. Zhou, Y. Shi, X. Zhu, Y. Yao, and J. Guo, Topologically nontrivial interband plasmons in type-II Weyl semimetal $MoTe_2$, New J. Phys. **22**, 103032 (2020).
[40] See Supplemental Material at http://link.aps.org/supplemental/10.1103/PhysRevB.109.144506 for additional information about the experimental discussion, which includes Refs. [28,30,35,41–45].
[41] T. Klimczuk, T. Plackowski, W. Sadowski, and M. Plebańczyk, A resistivity peak close to T_c in $Nd_{2-x}Ce_xCuO_{4-y}$ single crystals, Physica C: Superconductivity **387**, 203 (2003).
[42] D. Daghero and R. S. Gonnelli, Probing multiband superconductivity by point-contact spectroscopy, Supercond. Sci. Technol. **23**, 043001 (2010).
[43] M. D. Johannes, I. I. Mazin, and C. A. Howells, Fermi-surface nesting and the origin of the charge-density wave in $NbSe_2$, Phys. Rev. B **73**, 205102 (2006).
[44] T. Yokoya, T. Kiss, A. Chainani, S. Shin, M. Nohara, and H. Takagi, Fermi surface sheet-dependent superconductivity in $NbSe_2$, Science **294**, 2518 (2001).
[45] Y. Noat, J. A. Silva-Guillén, T. Cren, V. Cherkez, C. Brun, S. Pons, F. Debontridder, D. Roditchev, W. Sacks, L. Cario, P. Ordejón, A. García, and E. Canadell, Quasiparticle spectra of $2H$-$NbSe_2$: Two-band superconductivity and the role of tunneling selectivity, Phys. Rev. B **92**, 134510 (2015).
[46] C. Heikes, I.-Lin Liu, T. Metz, C. Eckberg, P. Neves, Y. Wu, L. Hung, P. Piccoli, H. Cao, J. Leao, J. Paglione, T. Yildirim, N. P. Butch, and W. Ratcliff, Mechanical control of crystal symmetry and superconductivity in Weyl semimetal $MoTe_2$, Phys. Rev. Mat. **2**, 074202 (2018).
[47] T. Le, L. Yin, Z. Feng, Q. Huang, L. Che, J. Li, Y. Shi, and X. Lu, Single full gap with mixed type-I and type-II superconductivity on surface of the type-II Dirac semimetal $PdTe_2$ by point-contact spectroscopy, Phys. Rev. B **99**, 180504(R) (2019).
[48] D. Zhang, T. Le, B. Lv, L. Yin, C. Chen, Z. Nie, D. Su, H. Yuan, Z.-A. Xu, and X. Lu, Full superconducting gap and type-I to type-II superconductivity transition in single crystalline $NbGe_2$, Phys. Rev. B **103**, 214508 (2021).
[49] F. Yang, Y. Ding, F. Qu, J. Shen, J. Chen, Z. Wei, Z. Ji, G. Liu, J. Fan, C. Yang, T. Xiang, and L. Lu, Proximity effect at superconducting Sn-Bi_2Se_3 interface, Phys. Rev. B **85**, 104508 (2012).
[50] W. L. McMillan, Tunneling model of the superconducting proximity effect, Phys. Rev. **175**, 537 (1968).
[51] K. Y. Yip, S. T. Lam, K. H. Yu, W. S. Chow, J. Zeng, K. T. Lai, and S. K. Goh, Drastic enhancement of the superconducting temperature in type-II Weyl semimetal candidate $MoTe_2$ via biaxial strain, APL Mater. **11**, 021111 (2023).
[52] C. Chen, D. Zhang, R. Kumar, Y. Zhang, G. Ye, L. Yin, J. Zhang, H. Yuan, C. Cao, and X. Lu, Tip-induced superconductivity enhancement in single-crystalline PdSb by point-contact spectroscopy, Phys. Rev. B **106**, 174520 (2022).
[53] J. Yang, J. Colen, J. Liu, M. C. Nguyen, G.-w. Chern, and D. Louca, Elastic and electronic tuning of magnetoresistance in $MoTe_2$, Sci. Adv. **3**, eaao4949 (2017).